International Journal of Thermophysics, Vol. 26, No. 2, March 2005 (© 2005)
DOI: 10.1007/s10765-005-4511-z

Measurement of the In-plane Thermal Diffusivity of Materials by Infrared Thermography[1]

B. Rémy,[2,3] A. Degiovanni,[2] and D. Maillet[2]

A transient method using the *Laplace* transform for estimation of the in-plane thermal diffusivity of low conductive materials is presented. The temperature field of the sample is measured by infrared thermography. The main interest of the technique proposed here is to not require a knowledge of the stimulation and boundary conditions by using two reference temperature profiles. The parameter estimation is implemented in the time domain by an inverse technique using numerical *Laplace* inversion and convolution products. A sensitivity study has been carried out to optimize the choice of the two reference profiles. The effect of a space varying heat transfer coefficient on the estimated values of the unknown parameters has also been evaluated. Finally, the apparatus is described and experimental results obtained for a low conductive material like a vitroceramic are shown.

KEY WORDS: infrared thermography; in-plane diffusivity; low conductive material; parameter estimation; transient technique.

1. INTRODUCTION

The fin's method in a transitory regime consists of studying the in-plane heat diffusion process within a sample with a small thickness e, compared to its extension L. The medium is assumed ideal (i.e., homogeneous, isotropic, and opaque) and initially at thermal equilibrium. The heat losses with the surroundings are taken into account by a constant heat transfer

[1]Paper presented at the Sixteenth European Conference on Thermophysical Properties, September 1–4, 2002, London, United Kingdom.

[2]Laboratoire d'Énergetique et de Mécanique Théorique et Appliquée — L.E.M.T.A — E.N.S.E.M — I.N.P Lorraine — U.M.R-C.N.R.S 7563 — U.H.P. Nancy I — 02, avenue de la forêt de Haye, B. P. 160, 54 516 Vandoeuvre-Lès-Nancy Cedex, France.

[3]To whom correspondence should be addressed. E-mail: bremy@ensem.inpl-nancy.fr

coefficient h. Also, we are making the assumption of uniform temperature distribution over the thickness of the material. Based on this principle, several methods have been developed and used to estimate the thermal diffusivity a of materials from in-time variations of the temperature field. The diffusivity is then obtained by either taking the ratio of two temperatures measured at a given position but at different times, or using the ratio of the in-time variations of two temperatures measured at different locations $x = x_1$ and $x = x_2$. This method has been used by Katayama et al. [1]. The main drawback of this technique is that the heat flux must be exactly known. Unfortunately, that is practically never the case in experiments. Then, it has been improved by Kavianipour and Beck [2] who showed that a knowledge of the heat flux function is not required if we are working in the *Laplace* domain.

This technique has been then extended by Hadisaroyo et al. [3] by taking into account both diffusivity and heat losses that cannot be neglected because of the natural fin's effect that naturally appears in materials with a large extension. The author proposed some in-space and in-time validation criteria and particularly showed that it was not necessary to have a uniform in-space stimulation if we consider the mean temperature calculated in the width direction. For the case of insulating materials and with the help of an infrared camera, it also showed that it was not necessary to take into account bidimensional effects if mean temperatures defined on two surfaces with large dimensions are considered. Finally, this method has been extended by Philippi et al. [4] for the estimation of the in-plane thermal diffusivity of anisotropic materials in a two-dimensional flash experiment through the temperature field of the rear-face sample measured by infrared thermography. Using *Fourier* transforms in space and a *Laplace* transform in time, it is then possible to not need information on the geometrical form of the excitation and on the precise location of the measurement points. The main disadvantage of this technique is that the stimulation must be a *Dirac* delta function in time. So, in the case of insulating materials, the heat diffusion effect is difficult to be observed. Indeed, before this effect appears, a large part of the energy deposited by the flash is lost through convection and when the measurement can be performed, there is insufficient energy in the material. To avoid this problem, we propose to generate an energy step. In this case, the *Laplace* transform of the experimental temperature field cannot be calculated because the energy of the signal we consider is not finite. To sort out this problem, we are staying in the time domain to make the measurement.

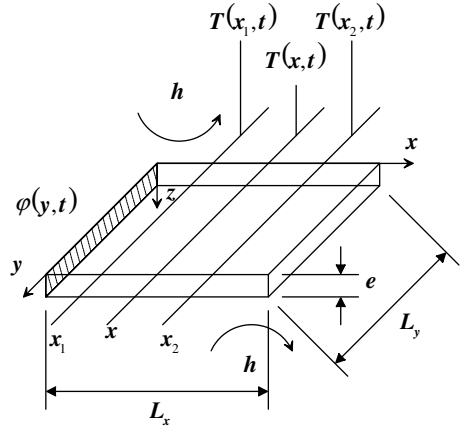

Fig. 1. Theoretical model.

2. PRINCIPLE OF THE MEASUREMENT

Let consider a finite medium in x and y directions and with a small thickness e compared to the sample expansions L_x and L_y (fin's approximation). To measure the thermal conductivity λ_x or diffusivity $a_x = \lambda_x/\rho C_p$, we stimulate the sample for $x=0$ by a nonessential uniform and constant heat flux $\varphi(y,t)$ or temperature step $T_0(y,t)$ (see Fig. 1) and consider the average temperature $\Delta\bar{T}(x,t) = \bar{T}(x,t) - T_{\text{ext}}$ in the y direction. Its expression is given by solving the following set of equations:

$$\frac{\partial^2 \Delta\bar{T}}{\partial x^2} - \frac{2h\,(e+L)}{eL}\frac{\Delta\bar{T}}{\lambda_x} = \frac{1}{a_x}\frac{\partial \Delta\bar{T}}{\partial t} \tag{1}$$

In the case where $e << L$, we have $\frac{2h(e+L)}{eL} \simeq \frac{2h}{e}$. Equation (1) represents the heat equation with a source term that takes into account the fin's effect (heat losses with the surrounding).

$$\text{for } x=0 \quad -\lambda_x \left.\frac{\partial \Delta\bar{T}}{\partial x}\right|_{x=0} = \bar{\varphi}_0(t) \quad \text{or} \quad \Delta\bar{T}\big|_{x=0} = \bar{T}_0(t) - T_{\text{ext}} \tag{2}$$

$$\text{for } x=L_x \quad -\lambda_x \left.\frac{\partial \Delta\bar{T}}{\partial x}\right|_{x=L_x} = \bar{\varphi}_L(t) \quad \text{or} \quad \Delta\bar{T}\big|_{x=L_x} = \bar{T}_L(t) - T_{\text{ext}} \tag{3}$$

$$\text{at } t=0 \quad \Delta\bar{T} = 0 \tag{4}$$

The solution can be easily obtained in the *Laplace* domain $(F(p) = L(f(t)) = \int_0^\infty f(t)\exp(-pt)dt)$ by using the quadrupole formulation (See

Ref. 5 for more details on this technique) that can be used to linearly link the *Laplace* transformed inner and outer temperatures $\theta = L(T)$ and fluxes $\Phi = L(\varphi)$ of the medium ($A_x = D_x = \cosh(kx)$, $B_x = \sinh(kx)/\lambda k$, $C_x = \lambda k \sinh(kx)$, and $k = \sqrt{p/a_x}$):

$$\begin{bmatrix} \theta_0 \\ \Phi_0 \end{bmatrix} = \begin{bmatrix} A_x & B_x \\ C_x & D_x \end{bmatrix} \begin{bmatrix} \theta_x \\ \Phi_x \end{bmatrix} = [M_x] \begin{bmatrix} \theta_x \\ \Phi_x \end{bmatrix} \quad \rightarrow \quad \begin{bmatrix} \theta_0 \\ \Phi_0 \end{bmatrix} = [M_e] \begin{bmatrix} \theta_e \\ \Phi_e \end{bmatrix} \tag{5}$$

By choosing two reference temperature profiles $T_1(t)$ and $T_2(t)$ in x_1 and x_2, we can show that all the other *Laplace* transformed temperature profiles $\theta(x, p)$ within the material can only be expressed as a linear combination of $\theta_1(p)$ and $\theta_2(p)$:

$$\theta(x, p) = \theta_1(p) F_1(x, p) + \theta_2(p) F_2(x, p) \tag{6}$$

with

$$F_1(x, p) = \frac{\sinh(\alpha(x_2 - x))}{\sinh(\alpha(x_2 - x_1))}$$

and

$$F_2(x, p) = \frac{\sinh(\alpha(x - x_1))}{\sinh(\alpha(x_2 - x_1))} \left(\alpha = \sqrt{p/a_x + 2h/e\lambda_x}\right)$$

Thus, an exact knowledge of the boundary conditions is not required. In the time domain, this can be written like the sum of two convolution products :

$$T(x, t) = T_1(t) \otimes f_1(x, t) + T_2(t) \otimes f_2(x, t) \quad \text{with } f_i(x, t) = L^{-1}(F_i(x, p)) \tag{7}$$

The temperatures $T_1(t)$ and $T_2(t)$ can be measured by an infrared camera. The analytical expressions of the functions $F_1(x, p)$ and $F_2(x, p)$ are exactly known, and the inverse transforms (Ref. 6) and convolution products are implemented by numerical algorithms. If we introduce the dimensionless quantities $x^* = x/L$, $t^* = at/L^2$, $p^* = pL^2/a$, $Bi = hL/\lambda$, and $\varepsilon = e/L$, these functions are given by

$$F_1(x^*, p^*) = \frac{\sinh(\alpha^*(x_2^* - x^*))}{\sinh(\alpha^*(x_2^* - x_1^*))} \quad \text{and} \quad F_2(x^*, p^*) = \frac{\sinh(\alpha^*(x^* - x_1^*))}{\sinh(\alpha^*(x_2^* - x_1^*))} \tag{8}$$

with $\alpha^* = \alpha L = \sqrt{p^* + 2Bi/\varepsilon}$. The functions f_1 and f_2 are plotted in Fig. 2 with $Bi = 0.4$ and $\varepsilon = 0.4$. If we take $x_1^* = 0$ and $x_2^* = 1$, then these functions are symmetric and they are equal for $x^* = 0.5$. So, we only have represented these functions for $0 \leqslant x^* \leqslant 1/2$. If $x^* \rightarrow x_1^* = 0$ then the

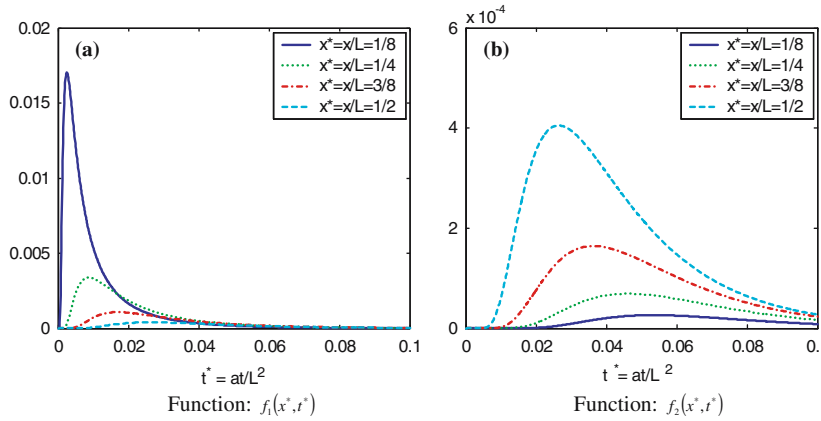

Fig. 2. Functions f_1 and f_2 versus reduced time t^* with $x_1^* = 0$ and $x_2^* = 1$.

maximum of the F_1-function is increasing and moving towards smaller times (the F_1-function tends to the *Dirac* function) while the maximum of the F_2-function is decreasing and moving to larger times (the F_2-function tends to the null function). Therefore, more weight is given to the first reference profile than to the second one. Due to the duality of these functions, this is naturally the opposite if $x^* \to x_2^* = 1$.

3. TEST CASE

To test the validity of the method we developed, we tried to estimate the unknown parameters from simulated temperature profiles. Our test case corresponds to a square sample ($L = 40$ mm and $e = 1$ mm) with the following thermophysical properties ($a = 5 \times 10^{-7} \mathrm{m}^2 \cdot \mathrm{s}^{-1}$, $\lambda = 1 \mathrm{W} \cdot \mathrm{m}^{-1} \cdot \mathrm{K}^{-1}$ and $h = 10 \mathrm{W} \cdot \mathrm{m}^{-2} \cdot \mathrm{K}^{-1}$) that is stimulated by a temperature step $\theta_0(p) = (T_0 - T_{\mathrm{ext}})/p$ for $x = 0$ and insulated for $x = L$. The solution of this problem can be easily obtained in the *Laplace* domain and is given by

$$\theta^*(x, p) = \frac{\theta(x, p)}{T_0 - T_{\mathrm{ext}}} = \frac{1}{p} \frac{\cosh(\alpha(x_2 - x))}{\cosh(\alpha(x_2 - x_1))} \tag{9}$$

The reduced steady-state temperature profile can be obtained by

$$\Delta T_\infty^*(x) = \lim_{p \to \infty} p.\theta^*(p) = \frac{\cosh(\alpha_0(x_2 - x))}{\cosh(\alpha_0(x_2 - x_1))}$$
$$\text{with} \quad \alpha_0 = \sqrt{2h/e\lambda_x} \simeq \sqrt{H} \tag{10}$$

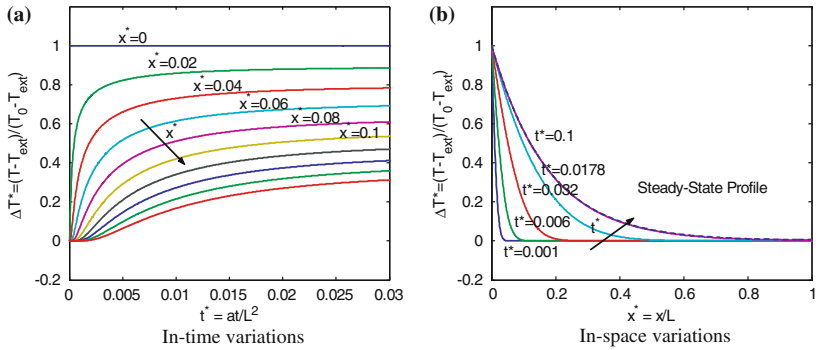

Fig. 3. In-time and in-space variations of the reduced temperature for the test case.

In Fig. 3 are given the in-time and in-space variations of the temperature profiles in dimensionless variables. Of course, we find that the steady-state profile (see Fig. 3b) tends to the fin's profile given by Eq. (10). The in-space temperature decay is a function of both the heat transfer coefficient and thermal conductivity of the material (see the expression of α_0). The estimation can be performed both with the in-space or in-time temperature profiles but in practice, we prefer to work with the in-time variations because the number of points in time are larger than the number of points in space. For a thermogram at a given position (see Fig. 3a), the steady-state value at larger times is a function of the heat transfer coefficient through the parameter α_0 and the time to reach this steady-state value is a function of the diffusivity of the material. In the inversion process that will be used in the next section, we are then going to estimate from these simulated thermograms the thermal diffusivity and heat transfer coefficient by assuming that the boundary conditions are now unknown.

4. PARAMETER ESTIMATION

The unknown parameters, the diffusivity a and heat losses $H = 2h(e+L)/(eL\lambda)$, are estimated by an inverse technique [7] based on an *ordinary least-squares method* (*OLS*) [8, 9] which consists of minimization of a sum S that represents the squared differences between the experimental $T_{\text{exp}}(t)$ and theoretical curves $T_{\text{the}}(t, \beta)$:

$$S = \sum_{i=1}^{n_t} \left(T_{\text{the}}(t_i, \beta) - T_{\text{exp}}(t_i) \right)^2 \tag{11}$$

$\beta = \begin{bmatrix} a \\ H \end{bmatrix}$ is a parameter vector composed of the unknown parameters β_j. The theoretical and experimental curves correspond to the thermograms over all the space domain $x_k = \frac{k}{n_x} L_x \; (k = 0, \ldots, n_x)$:

$$T_{\text{the}}(t_i, \beta) = \left.\begin{bmatrix} T_{\text{the}}(0, t_i, \beta) \\ \vdots \\ T_{\text{the}}(x_k, t_i, \beta) \\ \vdots \\ T_{\text{the}}(L_x, t_i, \beta) \end{bmatrix}\right\} \begin{matrix}(n_x+1) \\ \text{profiles}\end{matrix} \quad \text{and} \quad T_{\text{exp}}(t_i) = \begin{bmatrix} T_{\text{exp}}(0, t_i) \\ \vdots \\ T_{\text{exp}}(x_k, t_i) \\ \vdots \\ T_{\text{exp}}(L_x, t_i) \end{bmatrix} \tag{12}$$

Minimizing S with respect to β_j is equivalent to making its derivatives equal to zero.

$$\frac{\partial S}{\partial \beta_j} = 0 \rightarrow \sum_{i=1}^{n_t} \frac{\partial T_{\text{the}}(t_i, \beta)}{\partial \beta_j} \left(T_{\text{the}}(t_i, \beta) - T_{\text{exp}}(t_i)\right) = 0 \quad (\forall j) \tag{13}$$

A sensitivity matrix denoted as X naturally appears in the optimization process and plays a key role in the estimation process. Each element X_{ij} represents the derivative of the signal with respect to the parameter β_j at time t_i, and each column represent the sensitivity curve or sensitivity coefficient for a given parameter. By a linear expansion of the model around the solution and by assuming that the noise on the experimental curve is additive

$$T_{\text{exp}}(t_i) = T_{\text{the}}(t_i, \beta) + \varepsilon(t) \tag{14}$$

with $\varepsilon(t)$ the noise at time t.
We can obtain an analytical relation between the estimated values of the parameters denoted as $\hat{\beta}$ and their real values β:

$$\hat{\beta} = \beta + \left(X^t X\right)^{-1} X^t \varepsilon(t) \tag{15}$$

We then commonly make the assumption of a random and noncorrelated noise that follows a normal distribution with a mean value $E(\varepsilon) = 0$ and a constant variance $V(\varepsilon) = \sigma_b^2$ (σ_b being the standard deviation of noise). Under these assumptions, we can show that the expected values of parameters are given by

$$E\left(\hat{\beta}\right) = \beta \qquad \text{(unbiased estimator)} \tag{16}$$

and the variance/covariance of parameters $\sigma_a^2 = \sigma_b^2 \operatorname{Var}(a)$ and $\sigma_H^2 = \sigma_b^2 \operatorname{Var}(H)$ by

$$V\left(\hat{\beta}\right) = \sigma_b^2 \left(X^t X\right)^{-1} = \sigma_b^2 \begin{bmatrix} \operatorname{Var}(a) & \operatorname{Cov}(a, H) \\ \operatorname{Cov}(a, H) & \operatorname{Var}(H) \end{bmatrix} \tag{17}$$

We define the correlation factor as

$$\rho(a, H) = \frac{\operatorname{Cov}(a, H)}{\sigma_a \cdot \sigma_H} \tag{18}$$

The relation given in Eq. (15) is very important because it allows us to evaluate the errors in the estimated parameters. Equation (17) clearly shows that if the signal is not corrupted by the measurement noise, one can expect to estimate the parameters with a high accuracy, even if their effects on the signal are strongly coupled. In contrast, in the case of a noisy signal, errors in the values of the estimated parameters directly depend on the noise level, particularly if they are strongly coupled. A given parameter will be then well estimated if its sensitivity curve is large and noncorrelated with another one. These two aspects are both taken into account through the variance–covariance coefficients (i.e., standard deviations) in the inversion process. This will be specifically discussed in the next section. In our case, Eqs. (16) and (17) are not rigorously exact because the theoretical model has noise through the two reference profiles that have been chosen.

$$\begin{aligned} T_{\text{the}}(x_k, t_i, \beta) = {} & T_{\text{the}}(x_k, t_i, \beta)|_{\varepsilon_1=\varepsilon_2=0} + \varepsilon_1(t_i) \otimes f_1(x_k, t_i) \\ & + \varepsilon_2(t_i) \otimes f_2(x_k, t_i) \end{aligned} \tag{19}$$

where $\varepsilon_1(t)$ and $\varepsilon_2(t)$ represent noise in the reference profiles for $x = x_1$ and $x = x_2$ with the same properties as $\varepsilon(t)$. Then, this is a rough approximation to make the assumption of noise with a normal distribution in Eq. (15). Nevertheless, these relations are still of interest because we can show that in our model, the standard deviations remain a function of the $\left(X^t X\right)^{-1}$ matrix that appears in Eq. (17) in the ideal case.

4.1. Optimal Choice of the Reference Profiles

The main difficulty in this problem is in the selection of the two reference profiles. The natural choice is to take them for $x = 0$ and $x = L_x$. In this section, we are going to show through a sensitivity study and standard deviations calculation that this choice appears to be the optimal one. In Fig. 4 are plotted the sensitivity curves for a and H. Figure 4a corresponds to the sensitivity curves obtained from the direct model given by

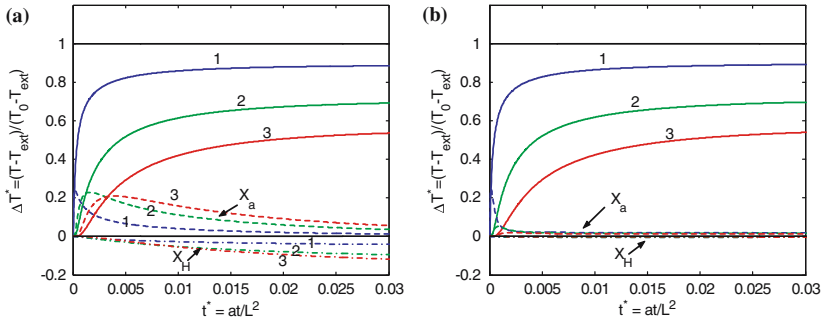

Fig. 4. Sensitivity curves for a and H in the two limiting cases.

Eq. (9). We also have drawn the same curves from the general model given by Eq. (6) by choosing the reference profiles for $x_1 = 0$ and $x_2 = L$. Theses curves are not represented here because the results we obtained are strictly the same as those given by the direct model. This can be explained by the fact that the reference profiles are insensitive to the unknown parameters because the temperature is constant for $x_1 = 0$ and is equal to zero for $x_2 = L$. These profiles could have been chosen in other ways. For instance, to compute the in-time variation of the temperature in x_k, we could let $x_1 = 0$ and $x_2 = x_{k+1}$, or $x_1 = x_{k-1}$ and $x_2 = L$ (one moving reference profile), or even $x_1 = x_{k-1}$ and $x_2 = x_{k+1}$ (two moving reference profiles). The results in terms of correlation and standard deviations are given in Table I for thermograms with 1000 points in time and for 50 equally spaced positions, but, for more clarity, only a few of them have been plotted in Fig. 4. We have also represented only the sensitivity curves in the case of the two moving reference profiles method (see Fig. 4b) because the others have an intermediate behavior between the two limiting cases presented here. We can notice that if the reference profiles are close to the calculated profile then the maximum of the sensitivity curves for parameter a is decreasing. The closer the reference profiles, the lower is the maximum. So it is for the sensitivity curves for H that tend to zero. This can be explained by the small differences that appear between the succeeding thermograms for x_{k-1}, x_k and x_{k+1}. Especially, over such a small distance, the fin's effect that appears in the material cannot be revealed.

4.2. Effect of a Nonuniform Heat Transfer Coefficient

In practice, the sample is held in a vertical position to perform the measurement of the temperature field with an infrared camera. So, if the

Table I. Variance-Covariance to a and H for Different Reference Profiles

	Var(a)	Var(H)	Cov(a, H)	ρ (a, H)
Direct model	0.011	0.036	0.015	0.743
General model				
$x_1 = 0,\ x_2 = L$	0.011	0.036	0.015	0.743
$x_1 = 0,\ x_2 = x_{k+1}$	0.090	0.397	0.106	0.562
$x_1 = x_{k-1},\ x_2 = L$	0.135	0.529	0.180	0.676
$x_1 = x_{k-1},\ x_2 = x_{k+1}$	0.882	24.389	3.652	0.787

material is heated on its bottom or top sides, the heat transfer coefficient varies with respect to the space variable whereas the theoretical model we use only accounts for a constant heat transfer coefficient. This effect can be reduced if the sample is stimulated from the side—that which we do experimentally—but it is crucial to know if the estimation of the diffusivity can be affected by such an effect. To answer this question, we simulated the heat transfer in the square sample using a finite element software (*FlexPDE*©). Two cases have been considered: a constant and an in-space varying heat transfer coefficient. The in-space variation of the heat transfer coefficient we used is given by the following relation:

$$h(x) = \frac{3}{4} h_0 \left(\frac{L}{x}\right)^{1/4} \tag{20}$$

It has been chosen in such a way its mean value $\bar{h} = \frac{1}{L}\int_0^L h(x)\,dx$ is equal to the value of the constant heat transfer coefficient h_0. The thermograms we obtained by taking the column-wise average of the temperature field are plotted in Fig. 5. We can observe that the maximum temperature is lower in the case of a nonuniform coefficient than in the case of a constant one. This can be easily explained by the fact that the local value of the heat transfer coefficient is higher near the hottest zone. (see Eq. (20)). Then, the diffusivity a and heat losses through parameter H have been estimated in the two cases we considered. The nominal values of these parameters are equal to $a = 5 \times 10^{-7} \mathrm{m}^2 \cdot \mathrm{s}^{-1}$ and $H = 20,500$ ($h = 10\,\mathrm{W} \cdot \mathrm{m}^{-2} \cdot \mathrm{K}^{-1}$ and $\lambda = 1\,\mathrm{W} \cdot \mathrm{m}^{-1} \cdot \mathrm{K}^{-1}$), respectively. The experimental and theoretical curves which are computed with the estimated values are shown in Fig. 6. Only a few of them are represented, but the estimation was performed with 1000 points in time and 50 profiles in space. The reference profiles are taken for $x_1 = 0$ and $x_2 = L$. In the case with $h = h_0$, the estimated values are very close to the nominal values ($a = 4.98 \times 10^{-7} \mathrm{m}^2 \cdot \mathrm{s}^{-1}$

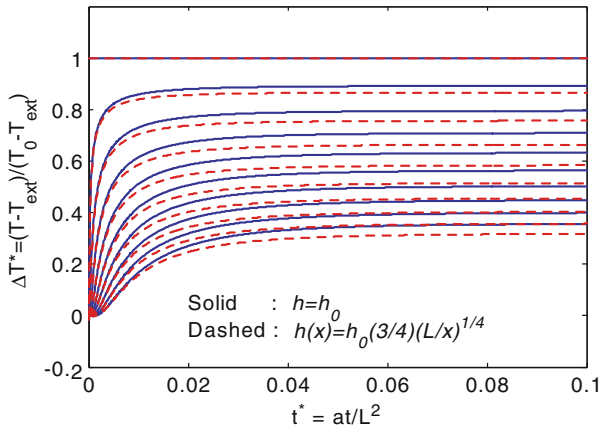

Fig. 5. Thermograms with uniform and nonuniform heat transfer coefficients.

compared to $a = 5 \times 10^{-7} \mathrm{m}^2 \cdot \mathrm{s}^{-1}$ and $H = 20,422$ instead of $20,500$ or $h = 9.96 \,\mathrm{W} \cdot \mathrm{m}^{-2} \cdot$ K instead of $10 \,\mathrm{W} \cdot \mathrm{m}^{-2} \cdot \mathrm{K}^{-1}$). The small differences can be explained by numerical errors due to the numerical solver. In the case of a space-varying heat transfer coefficient, the small discrepancies between simulated and calculated curves clearly show that the in-space variations can only be taken into account by a mean heat transfer coefficient with no apparent effect on the estimated value of the diffusivity that kept the same value. Thus, this demonstrates the reliability of the method for the case of a nonuniform heat transfer coefficient. The large estimated value of $H = 25456$ ($h = 12.42 \,\mathrm{W} \cdot \mathrm{m}^{-2} \cdot$ K) compared to the mean value h_0 can be explained by the fact that the local values of h are greater in the first part of the material than in the second part.

5. EXPERIMENTAL RESULTS

In this section, results obtained on a vitroceramic are presented. The apparatus is very simple and is composed of a square material (40 mm $\times$ 40 mm) with a thickness of 1 mm. The sample is held in a vertical position and is stimulated by a heating element on a vertical side to reduce the effect of free convection. The establishment of the fin's temperature profile within the material is then considered (see Fig. 7a) and measured by an infrared camera *AGEMA* 782SW cooled by liquid nitrogen and composed of an *InSb* detector sensitive in the wavelength range, [3.5–5.6 μm]. The acquisition frequency is equal to 6.25 Hz and only 1 image over 8 is recorded. The film is set at 256 images with a duration of 327.68 s, and

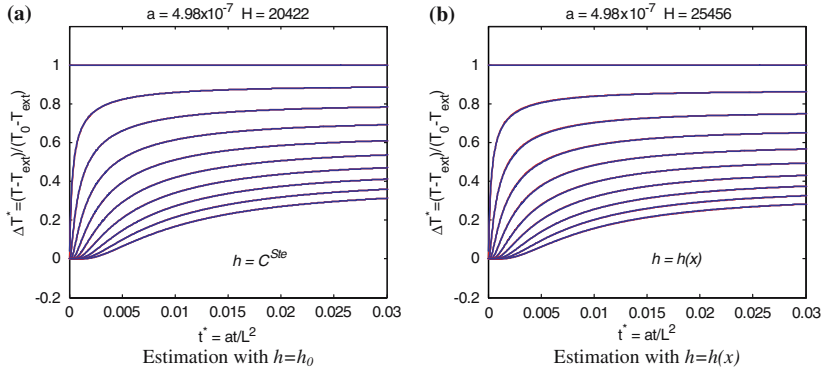

Fig. 6. Experimental and theoretical curves for the cases $h = C^{ste}$ and $h = h(x)$.

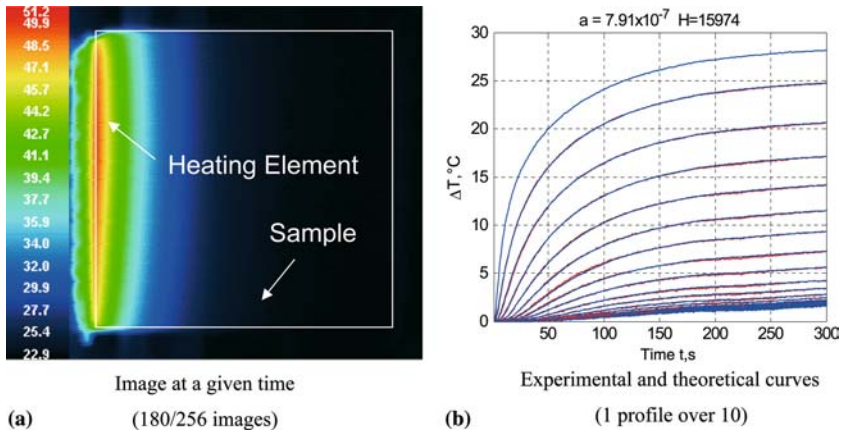

Fig. 7. Experimental results on a vitroceramic.

each image is composed of 280 lines and 280 columns. The value of the diffusivity obtained by this method ($a = 7.91 \times 10^{-7} \mathrm{m}^2 \cdot \mathrm{s}^{-1}$) on an isotropic material is very close to the diffusivity measured through the thickness of the same material by the classical *flash* method ($a = 7.85 \times 10^{-7} \mathrm{m}^2 \cdot s^{-1}$) (Ref. 10 and ASTM Standard E1461-92) and demonstrates the reliability of this technique.

6. CONCLUSION

This method appears to be very efficient in measuring in-plane diffusivities of materials and can be extended very easily for the characterization

of orthotropic materials (The diffusivity in each direction can be obtained from two independent experiments after a tilt of 90° of the sample). The main interest of this technique is to be nonintrusive and to not require knowledge of the in-time and in-space shapes of the excitation and of the precise location of the measurement points. Compared to the in-plane flash technique, this method is more sensitive (larger temperature variations) and allows the continuous introduction of energy in the material to perform measurements on low conductivity materials. Finally, the great quantity of experimental data produced by the infrared camera enables improvement of the accuracy of the parameters that are estimated.

REFERENCES

1. K. Katayama, *Bull. J.S.M.E.* **12**:865 (1969).
2. A. Kavianipour and J. V. Beck, *Int. J. Heat Mass Transfer* **20**:259 (1977).
3. D. Hadisaroyo, J. C. Batsale, and A. Degiovanni, *J. Phys. III*: 111 (1992).
4. I. Philippi, J. C. Batsale, D. Maillet, and A. Degiovanni, *Rev. Sci. Instrum.* **1**:182 (1995).
5. D. Maillet, S. André, J. C. Batsale, A. Degiovanni, and C. Moyne, *Thermal Quadrupoles—Solving the Heat Equation Through Integral Transforms* (Wiley, Chichester, 2000).
6. F. R. De Hoog, J. H. Knight, and A. N. Stokes, *S.I.A.M J. Sci. Stat. Comput.* **3**:357 (1982).
7. J. V. Beck and K. J. Arnold, *Parameter Estimation in Engineering and Science* (Wiley, New York, 1977).
8. K. Levenberg, *Quart. Appl. Math.* **2**:164 (1944).
9. D. Marquardt, *S.I.A.M. J. Appl. Math.* **11**:431 (1963).
10. W. J. Parker, R. J. Jenkins, C. P. Butler, and G. L. Abbott, *J. App. Phys.* **32**:1679 (1961).